Materiales de Construcción 75 (358)
April-June 2025, e376
ISSN-L: 0465-2746, eISSN: 1988-3226
https://doi.org/10.3989/mc.2025.380024

Surface crack detection on strengthened concrete beams using digital image processing

R.Kirthiga, S. Hariny, R. Javad, S. Elavenil ✉

School of Civil Engineering, Vellore Institute of Technology, (Chennai, India)
✉: elavenil.s@vit.ac.in

Received 19 March 2024
Accepted 11 October 2024
Available on line 04 September 2025

ABSTRACT: Fabric Reinforced Cementitious Matrices (FRCMs) are effective for strengthening reinforced concrete structural members. This study investigates beam load-carrying capacity of the strengthened beam pre-pre-loaded to 25%, 50%, and 100% with control beam. Subsequently, the beams were strengthened with single, double, and three layers of glass fabrics using cement binder. Results showed that the beams pre-loaded with 25% and 50% increased in load-carrying capacity of strengthened beam with Glass Fabric Reinforced Cementitious Matrix (GFRCM). Beams pre-loaded with 100% increased the load capacity for the double and three layer of GFRCM. Deflection for all strengthened beams decreased, except the 100% pre-loaded beam with single layers. Finite element analysis (FEA) was used to model the strengthened beam, and results were compared with experimental results. Image processing techniques were adopted to identify the surface cracks that developed on the strengthened beams and ascertain the features of the cracks.

KEY WORDS: Concrete beams; Finite element analysis; Fabric reinforced cementitious matrix; Image processing techniques; Load-carrying capacity; Deflection.

Citation/Citar como: Kirthiga R, Hariny S, Javad R, Elavenil S. 2025. Surface Crack Detection on Strengthened Concrete Beams using Digital Image Processing. Mater. Construcc. 75(358):e376. https://doi.org/10.3989/mc.2025.380024

RESUMEN: *Detección de fisuras superficiales en vigas de hormigón reforzado mediante procesamiento de imágenes digitales.* Las matrices cementíceas reforzadas con tela (FRCM) son efectivas para fortalecer miembros estructurales de hormigón armado. Este estudio investiga la capacidad de carga de la viga reforzada precargada al 25%, 50% y 100%, con la viga de control. Las vigas se reforzaron con una, dos y tres capas de tela de vidrio utilizando ligante de cemento. Los resultados mostraron que las vigas precargadas al 25% y 50% aumentaron su capacidad de carga con la matriz cementícea reforzada con tela de vidrio (GFRCM). Las vigas precargadas al 100% aumentaron la capacidad de carga con capas dobles y triples de GFRCM. La deflexión disminuyó en todas las vigas reforzadas, excepto en la viga precargada al 100% con una sola capa. Se utilizó el análisis de elementos finitos para modelar las vigas reforzadas y comparar los resultados con los datos experimentales. Se adoptaron técnicas de procesamiento de imágenes para identificar y caracterizar las grietas superficiales en las vigas reforzadas.

PALABRAS CLAVE: Vigas de hormigón; Análisis de elementos finitos; Matriz cementosa reforzada con tela; Técnicas de procesamiento de imágenes; Capacidad de carga; Deflexión.

1.INTRODUCTION

Developing novel strengthening and repair methods for reinforced concrete (RC) structures is essential, particularly in seismic-prone areas where the ductility of the structure plays a key role in determining the best strengthening strategy (1). Numerous studies have examined the strengthening of concrete beams using externally bonded Fiber Reinforced Polymer (FRP) composites(2). FRPs have superior mechanical properties, with an immense strength-to-weight ratio, elastic modulus, and corrosion resistance (3). To improve the structural behavior of reinforced members under accessibility and ultimate circumstances, fabrics or laminates are bonded externally to the surface of reinforced concrete members using epoxy as a bonding material (4). The use of epoxy for bonding fabrics and concrete has many benefits, as it is an excellent glue material and effective at transferring load to the fabric (5). However, it has many drawbacks, such as a lack of permeability, inadequate resistance to fire, elevated temperatures, and poor resistance to ultraviolet radiation (6).These drawbacks cause the external bonds to degrade and impair the strength of defective beams (7). To overcome these limitations, cement mortar used as a binder for FRP with concrete surfaces is referred to as a Textile Reinforced Mortar (TRM) or Fabric- reinforced cementitious matrix (FRCM) (7, 8).

FRCM has been successfully deployed for RC structural members using a wide range of strengthening techniques for RC structural members (9). Such methods include flexural/shear strengthening of beams (10, 11) or slabs (12, 13), confinement of concrete columns (14,15), and seismic strengthening of structures (16, 17). In most cases, the FRCM technique is highly effective in enhancing the strength and deformation properties of strengthened components (18). FRCMs can compete with FRPs in terms of performance if appropriate mortar-to-concrete and mortar-to-fabric bond conditions are attained (19). Ombres et al. investigated a RC beam strengthened with an FRCM by varying the fabric layers and noted that the strengthened beam increased the yielding and load-carrying capacity compared to the control beam. Moreover, the ductility of reinforced concrete beams decrease with an increase in the reinforcement ratio owing to concrete crushing and delamination of the fabric (20). Ambrisi et al. evaluated a beam strengthened with a Polyphenylene Benzobisoxazole (PBO) fabric embedded in two distinct types of commercially available cement mortar. They found that mortar with superior mechanical qualities resulted in a 38% higher load-carrying capacity and changed the failure mechanism of concrete-mortar from interlaminar shearing to debonding (21). Babaeidarabad et al. examined the bending behavior of concrete beams reinforced using PBO-FRCMs. They found that by increasing the fabric layers, the strength increased from 13% to 93%, and fabric slippage and delamination failures were observed (22). Increasing the number of fabric layers of FRCM changes the modes of failure from crushing to slippage of the fabric from the matrix (23,24). Awani et al. varied the reinforcing ratio in FRCM composites to strengthen RC beams in terms of shear strength. Researchers have revealed that FRCM composites increase beams shear strength by 51% to 145%. In addition, they observed that the shear strength of the beam increased non-proportionally with an increase in fabric layers (25). According to Loreto et al., increasing the volume percentage of the textiles improves the load-carrying capacity of RC slabs (26). Focacci et al. showed that the fabric type and bond at the fabric-matrix interface determines the strengthening efficacy of FRCM composite (27). The flexural capacity of an RC-strengthened beam with Basalt-FRCMs increased, and no slippage was found between the reinforced fabric layers and also observed the fabric rupture, and crushing of concrete failure (28). Moreover, a U-shaped strengthening configuration is one of the best anchorage techniques for delaying the debonding failures at the end of an FRCM matrix (29). Moreover, adopting the U-wrap as a strengthening technique increases the ultimate capacity and service life of the strengthened beams. Tarunkumar et al. studied the effect of industrial waste to increase the mechanical and microstructural properties (28)(29).

Cracks on the surface of a structure are the primary indicators of the health of a building, particularly in RC structures (30). Concrete is highly susceptible to cracking owing to its inherent weakness under tension (31). Cracking is one of the main causes of deformation, leading to the collapse of concrete structures (32). Moreover, cracks on the concrete surface permit moisture through the pores formed in the concrete, which may threaten the serviceability of RC structures (33). Assessing the level of damage by measuring the lengths of cracks is essential for engineers to prepare a budget for repairing damaged RC structures (34). This evaluation helps determine appropriate retrofitting techniques for renovation projects. In addition, it allows engineers to precisely calculate project expenses (33). Civil engineering industries have employed several effective techniques to determine and assess damage levels in RC structures. Several efficient methods have been employed to detect and assess the damage levels in RC structures, including visual, fiber optic-methods, and ultrasonic techniques (35). Skilled inspectors perform visual inspection at the crack scale. However, this is an extremely quantitative, subjective, laborious, and time-consuming method (36). Image-based crack detection, also known as image processing, has rapidly grown and been successfully applied to civil structures. To examine pavement cracks, Li et al. presented the grey theory and developed enhanced image pre-processing techniques using a segmentation algorithm (37). The crack thickness crack thickness was measured by Jahanshahi et al. using a depth-perception technique. This approach was well suited for integration with fully or partially autonomous mobile inspection systems (38).

This study examines the behavior of strengthened concrete beams using a Glass Fabric Reinforced Cementitious Matrix (GFRCM). The concrete beams were pre-loaded with three levels of damage before being strengthened with GFRCM. The experimental test results reported the ultimate load, deflection, and percentage increase in load. In an addition, this study presents a numerical method for calculating the deflection of concrete beams strengthened with FRCM. Furthermore, image-processing techniques for identifying surface cracks on strengthened beams and defining crack features are provided.

2. EXPERIMENTAL PROGRAM

2.1. Concrete beams

Ten prismatic specimens were cast, including the control specimen which had a length of 500mm and a cross-sectional area of 100mm x 100mm. A mix design, according to 10262:2019 (36), was formulated for the M30 grade concrete. Three concrete cubes were cast and tested after 28 days of curing, and they achieved a compressive strength of 35.46 MPa with a standard deviation of 1.98. Figure 1 shows the prismatic concrete specimen after curing for 28 days.

2.2. Strengthening material components

2.2.1. Mortars

Cement, silica fumes (SF), bagasse ash (SCBA), PVA fibers, and river sand were used as binders for the FRCM. As per IS 269:2015, OPC 53 grade Chettinad cement was used. Bagasse ash was sourced from the Kothari sugar industry in the Ariyalur district, Tamil Nadu, India. Upon obtaining the bagasse ash, it was dried in an oven for 24 hours and then sieved using a 75µ sieve. SF was purchased from a commercial supplier. A Poly-carboxylate based super plasticizer was used to achieve the desired consistency. Table 1 lists the physical properties of the binders.

Figure 1. Prismatic concrete specimen.

Table 1. Physical properties of the binder.

Properties	SF	OPC	SCBA	Sand
Specific gravity	2.2	3.14	2.67	2.65
Surface area (m^2/g)	3.8641	3.360	25.59	-
Initial setting time (min)	-	75	-	-
Final setting time (min)	-	365	-	-
Consistency (%)	-	31	-	-

To determine the mechanical properties of the binder used for FRCM, cement mortar cubes and mortar prisms were cast according to EN 1015-11, and the compressive and flexural strengths of the cement- binder were measured. The specimens were tested after 28 days of water curing, with a compressive strength of 61.79 MPa and flexural strength of 10.15 MPa (39).

2.2.2. FABRIC

An alkali resistant (AR)-glass fabric grid was considered as the strengthening material in this study. The spacing and thickness of the grid were measured as 3mm and 0.035mm, respectively. Tensile tests were performed on the AR-glass fabric strip according to ISO 10618:2004 (40). The fabric strip was not saturated with the cement-based binder and had dimensions of approximately 300mm x 40mm.To avoid specimen failure at the ends, fabric grids were bonded using epoxy to increase the grip during the tensile tests. The properties of the AR-glass fabrics are listed in Table 2 with average value and co. efficient of variance (COV).

Table 2. Concrete mixes used in the study.

Properties	Average value	COV
Tensile strength of the fabric grid(MPa)	1121	2.1
Cross sectional area (mm^2)	1.4	1.42
Tensile strength of yarn in the warp direction (MPa)	1233	3.2
Tensile strength of yarn in the weft direction (MPa)	1120	2.4
Length of the PVA fibers (mm)	6	-
Diameter of the PVA fibers (µm)	24	-

2.3. Pre-cracking beams

The beams were pre-loaded before applying the FRCM techniques. A three-point loading was applied to determine the ultimate capacities of the beams. Three pre-cracking levels were applied to the concrete beam, corresponding to 100%, 50%, and 25% of the yield load of the control beam. The yield load of the control beam was measured as 8.04 kN.

2.4. Strengthening application

The pre-cracked beams were repaired with cement paste, and the concrete surfaces were roughened using sandpaper to ensure the better bonding between the concrete surface and FRCM. The beams were strengthened using U-wrapping. After surface preparation, the concrete substrate was initially coated with a cement-based binder, followed by slight pressing of the glass fabric into the mortar. The second coating layer was then applied to complete the strengthening techniques. This process is repeated until the required number of fabric layers is obtained. All strengthened beams underwent a seven days curing period in the laboratory, before testing. Figures 2(a) and 2(b) shows a schematic diagram of the proposed strengthening techniques (U-wrap) and the strengthening of concrete beams with GFRCM, respectively.

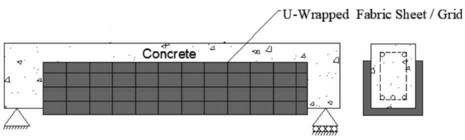

(a)

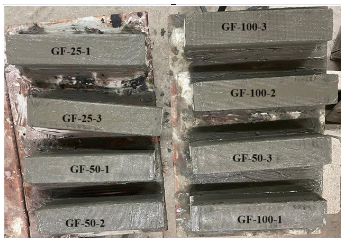

(b)

Figure 2. (a) Schematic diagram for strengthened beam with U-wrap (6); (b) Strengthening of the beam using GFRCM.

2.5. Testing of the strengthened beams

All strengthened beams were tested under point loading, as shown in Figure 3. The supports were composed of metal cylinders that allowed the specimens to rotate freely within the beam plane. Experiments were conducted using a hydraulic controller with a 500kN maximum capacity under displacement control at a speed of 1mm/min. A load was applied at the mid-span of the specimen until failure.

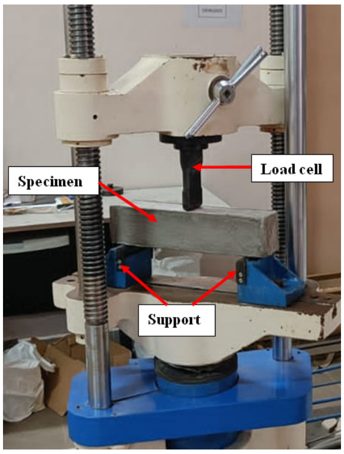

Figure 3. Experiment Test setup.

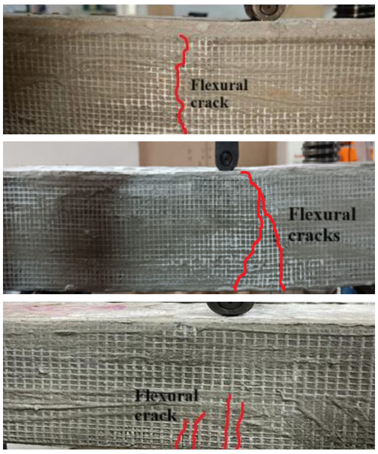

(a)

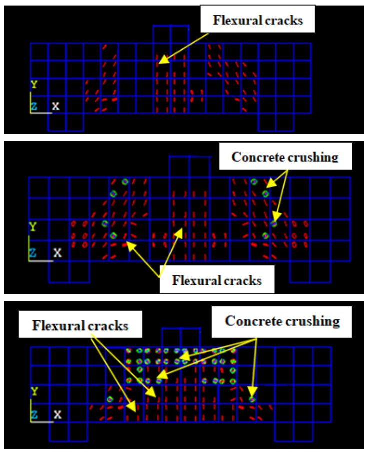

(b)

Figure 4. (a) Experimental failure modes; b) Numerical failure modes.

All specimens were deflected at the mid-span of the concrete beams, and small cracks developed in the specimens GF-25-1 and GF-25-2. The specimens pre-cracked up to 100% and 50% exhibited crack development towards the top surface of the specimens. This crack development occurs because of the significant loss of strength before strengthening. Beams strengthened with three layers' experience micro-cracking or more pronounced crack propagation within the GFRCM or the concrete, leading to increased deflection compared to those with one or two layers. The failure mode for the strengthened beams with two and three layers of fabric involved the formation of flexural cracks at the mid-span, which abruptly opened owing to fabric rupture. Large flexural cracks were observed in the specimens strengthened with a single layer, and debonding failure was observed in GF-100-3 and GF-50-3. Concrete crushing was noted in the specimen GF-100-2 and GF-100-3 with the fabric slippage. Figure 4(a) and (b) shows the failure modes of strengthened beams. Beams strengthened with one or two layers of GFRCM exhibit less deflection than those with three layers. This was due to the improved stiffness and crack resistance provided by the fabric layers. The crack pattern for the strengthened beam was observed using ANSYS. The model was converted to Mechanical APDL to accurately note the crack pattern for the strengthened beam.

3. EXPERIMENTAL RESULTS AND DISCUSSION

The results of each tested beam are listed in Table 3 considering their maximum load capacity, percentage of increasing load, and mid-span deflection.

Table 3. Experimental test results.

S.No	Damage level (%)	Specimen	No. of layers	Ultimate load (kN)	% of increase in load	Maximum deflection (mm)
1	Control	C	-	8.04	-	1.324
2	25	GF-25-1	1	9.84	22.4	0.76
3		GF-25-2	2	10.06	25.12	1.15
4		GF-25-3	3	12.06	50	1.34
5	50	GF-50-1	1	8.65	7.59	0.69
6		GF-50-2	2	9.18	14.18	1.11
7		GF-50-3	3	11.34	41.04	1.33
8	100	GF-100-1	1	5.7	-29.1	0.51
9		GF-100-2	2	8.26	2.73	1.14
10		GF-100-3	3	8.93	11.07	1.43

The beam pre-loaded with a 25% yield load and, strengthened with a single layer attained an ultimate load of 9.84kN, which was 22.4% higher than un-strengthened beam, with a maximum deflection of 0.76 mm. Similarly, the beam strengthened with two layers reached an ultimate load of 10.06 kN, indicating an approximately 25.12% increase in load with a deflection 1.15 mm. The three-layered strengthened beam, attained a maximum load of 12.06kN, representing a 50% increase with a deflection of 2.8 mm. These findings suggest that the three-layered beams exhibited better strength characteristics at a damage level of 25%. Banjara et al. also noticed the similar findings for flexural deficient strengthened beam with carbon FRCM (41).

Further investigations were conducted to examine damage levels of 50% and 100%. In the case of 50% damage, as shown in Table 3, it can be concluded that for both 50% and 100% damage, the three-layered beam achieved the maximum ultimate load, with increases of 41% and 11.07% with a maximum deflections of 1.43 mm and 1.63 mm, respectively. In addition, the ultimate load capacity was reduced to full failure (100%) when strengthened with a single layer. It was observed that the ultimate load capacity of the strengthened beam for the 100% pre-loaded beam was lower than the other damaged levels. Beams strengthened with three layers experienced micro-cracking or more pronounced crack propagation within the GFRCM or concrete, leading to an increased deflection compared to those with one or two layers. The beams strengthened with one or two layers of GFRCM exhibited less deflection than those strengthened with three layers. Tan et al. (42) observed the similar results for pre-damaged beam strengthened with steel plate using ultra high performance concrete. This was because of the improved stiffness and crack resistance provided by the fabric layers. As the load increases, more cracks are developed and propagating towards the compression zone. Feng Yu et al. also confirmed similar findings for strengthened beams, observing the development of micro cracks at the bottom of the strengthened beams (4). Once the specimen achieves 60% of the load, shear cracks emerge closer to the supports and persist until the beam ultimately collapses (2). As the number of fabric layers increases, the load-carrying capacity of the strengthened RC beams exhibits a significant increase. This observation is agrees with the findings reported by koutas et al. (43). Therefore, it is recommended that FRCM can be used to strengthen concrete beams with damage levels between 25% and 50%.

4. FINITE ELEMENT MODELLING

Finite element analysis is a numerical approach, which provides solutions to problems that may be challenging to identify. In this study, numerical investigations were conducted using ANSYS software.

4.1. Concrete

The concrete was modeled using Solid 65, an eight-node solid element. These node elements feature three degrees of freedom, allowing translation in the X, Y, and Z directions. SOLID-65 can plastically deform, crush under compression, and crack under tension (39).

4.2. Modelling of FRCM

The FRCM composites were modeled using Solid 65 elements. To model the FRP composites in the beam model, Solid 185, and four noded shell elements were used. An element is defined by eight nodes with three degrees of freedom at each node. Using a 3-D solid element, namely Solid187, the support and application points of the load were modeled. The cement-based binder was also modeled using Solid 181 (44). The element CONTA173 models the connection between the beam and the FRCM techniques. It has four nodes and three translational degrees of freedom (DOFs). A multi-point constraint contact algorithm was used to define the interfacial behavior at the concrete-matrix interface under the assumption that it was entirely bound (41).

4.3. Results and discussion

4.3.1. Validation of numerical result

Finite element analyses of un-strengthened and strengthened concrete beams were performed using a loading-controlled method. Using these iteration methods, the maximum deflection of the specimen was computed and it is compared with the experimental results. Figure 5 and Figure 6 show the modeling meshing, equivalence, and deformation of the unstrengthened and strengthened concrete beams. The behavior of the strengthened beams was analyzed and compared with that of an un-strengthened beam. Figure 7 presents stress-deflection diagram for the pre-cracked strengthened beam and compares it with the unstrengthened beam.

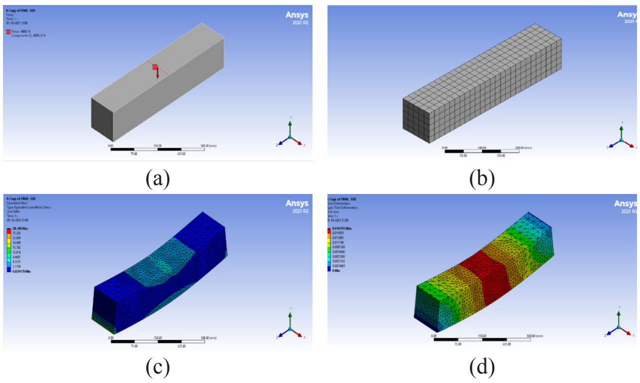

Figure 5. (a) Model of un-strengthened beam; (b) Meshing of un-strengthened beam; (c) Equivalent stress of un-strengthened beam and (d) Deformation of un-strengthened beam.

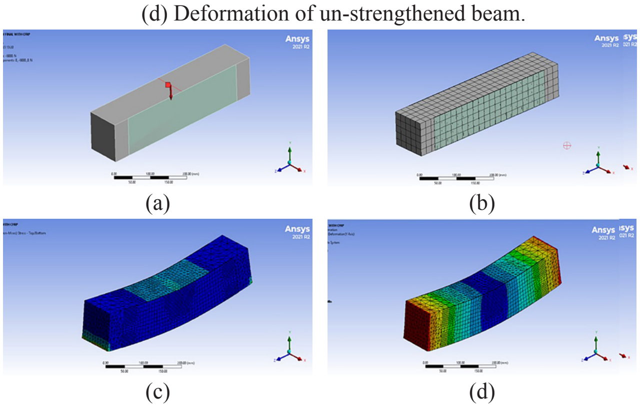

Figure 6. (a) Model of strengthened beam; (b) Meshing of strengthened beam; (c) Equivalent stress of strengthened beam, and (d) Deformation of strengthened beam.

From Figure 7, it can be seen that the deflections for the beam pre-loaded with 25% strengthening with one, two, and three layers were approximately 0.823, 1.203, and 1.45mm, respectively, which are higher than the experimental results. By increasing the percentage level of damage up to 50%, the strength increases, and deflections of approximately 0.8, 1.26, and 1.396mm were observed for beams with one, two, and three layers of strengthened concrete with FRCM, respectively. The full failure of the concrete beam strengthened with one, two, and three layers of FRCM enhanced the load-carrying capacity and attained minimum deflections of approximately 0.7, 1.165, and 1.476mm, respectively. Additionally, it was found that the FEA-derived deflection was approximately 10% lower than the experiment results. The failure modes of the un-strengthened beam in both experimental testing and FEA results exhibit strong concurrence, with the crushed concrete in the compression zone. In the experimental test, debonding and GFRCM failure happened first, followed by the beam matrix. Cracks in the strengthened specimens at failure were denser and smaller than those in the un-strengthened specimen, indicating that strengthened specimen reduced crack development (10).

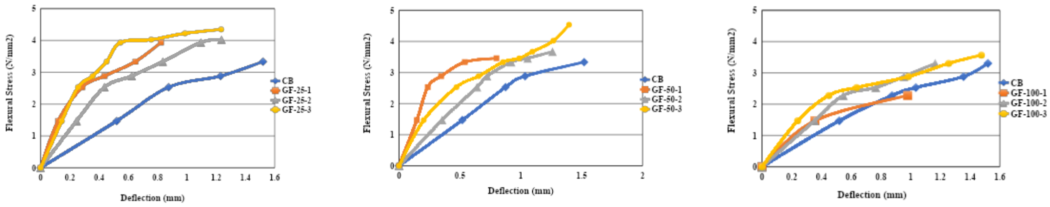

(a) (b) (c)

Figure 7. Stress-deflection curves for pre-cracked strengthened beams with damage levels of (a) 25%, (b) 50%, and (c) 100%.

The graph clearly shows that there was no sudden drop in load after the appearance of cracks in all strengthened beams during testing. These results are related to the contribution of glass-FRCM. Revanna et al. (45) also predicted the load-deflection graph, which show a similar respone and additionally, they observed that failure of GFRCM due to debonding. The viability of applying numerical simulations to predict the behavior of structures by changing the strength properties of concrete, force, and structural parameters, etc. is indicated by the strong correlation between the experimental and numerical data (46). This numerical model allows the prediction of not only the load and deflection of the concrete beams under external loading but also identifies the failure patterns (47).

5. IMAGE PROCESSING

To detect the crack features on the surface of the strengthened beam, the first step was to collect an image taken by a digital camera. These photographs contain excess information that must be deleted through pre-processing to make the crack detection process more effective.

5.1. Resizing

All the photographs were downsized to 256 × 256 pixels. With the loss of visual information, this phase promotes uniformity and accelerates the calculations. Additionally, the types of crack detection models that have been created thus far require scaled images for the models to properly function.

5.2. Grayscale Image Modification

Red, green, and blue (RGB) are the primary colors used for image recognition. The collected photos were processed to produce RGB and grayscale images. All the possible colors were produced by combining these three colors. The collected images contain several pixels with varying RGB channel values for every pixels, and these values helps to identify the cracks. The brightness level of the RGB images was changed to produce grayscale images. The grayscale image's brightness levels vary from 0 to 225, where 0 denotes black and 225 denotes white. The brightness (Y) of each pixel or amount of illumination is represented in the range of 0-225. To convert the RGB data into grayscale values, the MATLAB function that was used to builds a weighted sum of the individual RGB components. Figure 8 shows the crack and grayscale images.

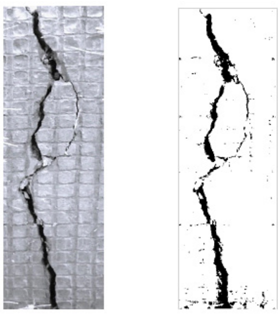

(a) (b)

Figure 8. (a) Image of the crack; (b) Grayscale image.

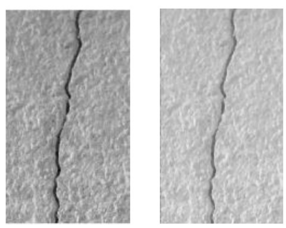

(a) (b)

Figure 9. (a) Normal image; (b) Denoised image.

5.3. Denoising

Noise is inevitably introduced into images for various reasons such as environmental factors (atmospheric conditions, lighting conditions, etc.,), transmission (data corruption, signal interface, etc.,), and compression algorithms. This noise may affect the clarity of the image, causing distortion and the loss of visual data. Noise interferes with the capacity of raw images to undergo image analysis, therefore, denoising is considered an essential pre-processing step (43). A two-dimensional median filter is employed to maintain the edges and remove noise. Compared to the raw grayscale image, the denoised background image was smooth, but the border attributes remained unchanged, as shown in Figure 9. The preprocessing techniques, such as resizing and denoising, used in this study are similar to those used by Golding et al., utilizing resizing for image standardization and median filtering to improve clarity. However, differences in edge detection algorithms might lead to variations in the observed crack features compared their results (48).

5.4. Sharpening

Sharpness is the contrast between two hues. A rapid transition from black to white can be observed in the Figure 10. However, the gradual transition from black to grey to white is hazy. Image sharpening refers to any enhancement technique that draws attention to edges and small details by increasing the contrast between bright and dark areas. The image is sharpened by masking, which subtracts the unsharp components of the image. To test the effects of sharpening, the grayscale intensity values of the pixels throughout the crack were noted at random location, as shown in Figure 10.

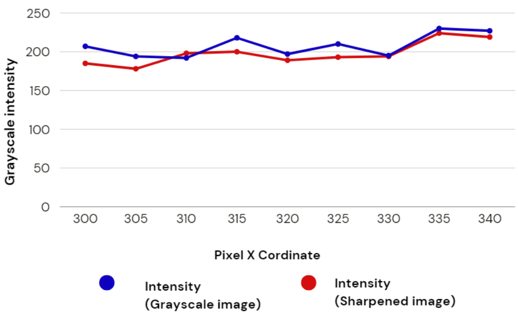

Figure 10. Grayscale intensity variations.

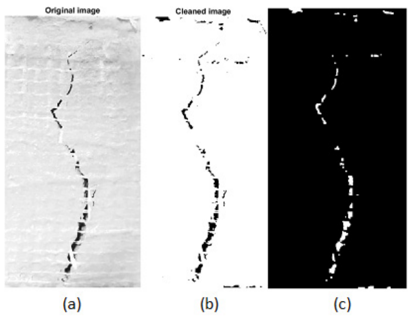

Figure 11. The detection of cracks (a) grayscale image; (b) edge image; (c) segmentation.

5.5. Edge detection

The computation of the gradient in an image serves as the foundation for edge detection. Wherever there is a sharp gradient, change in hue, or change in brightness, this procedure finds an edge. Edge detection and segmentation are two approaches to image analysis. Edge detectors are often mathematical techniques that can identify locations in an image where the intensity of gray levels exhibits discontinuities (30). In this case, an algorithm was used that can identify and remove spurious edges from mages (43), as shown in Figure 9.

Binarization algorithms in image processing convert grayscale or color images into binary images by thresholding pixel intensity values. These algorithms play a crucial role in various applications such as document scanning, object detection, and image segmentation. A binary picture alone can be represented as a matrix of 0's and 1's and is either entirely black or entirely white. MATLAB automatically converts all pictures to binary images while simultaneously recognizing edges (49).

Small areas of segmentations and edges may be caused by surface irregularities, such as cracks on rough surfaces in the processed images. Many morphological treatments were applied to the images to reduce the dispersion of these zones (50). However, patches cannot be removed using this technique. The final image, based on the edge detection and the segmentation approach is shown in Figure 11.

5.6. Crack attributes

Determining the crack attributes is the final stage of image processing. It is crucial to select characteristics that can quickly and easily distinguish noise from fracture. The major and minor axes are the longest overall lengths near the principal axis of any object that is closest to the centre of the main axis. This ensures that the specified object fully fits the ellipse created using these two dimensions. Both the horizontal and vertical orientations are recorded for each pixel. The pixels are recorded in the horizontal and vertical orientations. The maximum amount of bright pixels in a line should be increased by the number of cracks. The vertical and horizontal coordinates are used to categorize the cracks. If the vertical difference between the maximum and minimum coordinates of the cracks is less than 45 pixels, these cracks are classified as transverse cracks. Similarly, if the horizontal span between the highest and lowest coordinates is smaller than 45 pixels, the crack is classified as a longitudinal crack (51).

5.6.1. Crack length

Determining the location of a crack is the first step towards determining its length (52). Crack length is determined by measuring the extent of the crack along its longest axis (53). This is done by analyzing pixel coordinates to trace the crack's boundaries (54). The length is then calculated using these coordinates, often applying algorithms to ensure accurate measurements despite variations in image quality. Accurate crack length assessment helps evaluate the severity and progression of structural damage (30). The location of illuminated pixels on the lines is documented in both the horizontal and vertical orientations. Multiply the number of cracks by the maximum possible number of bright pixels in a line (55).

The crack lengths were calculated using MATLAB border function. The arrow-delineated limits of the crack were used to determine the crack length, which involved counting the pixels along the path of the crack (A, B, C, D). The crack lengths measured in our study, reaching up to 221 pixels, align with those reported by Senin et al. and found crack lengths of up to 220 pixels (33). Figure 12 shows the crack length measurements.

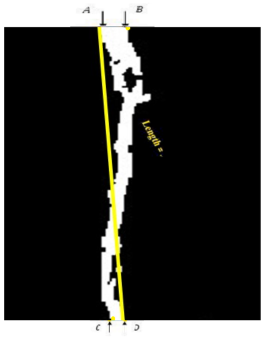

Figure 12. Measurement of the crack length.

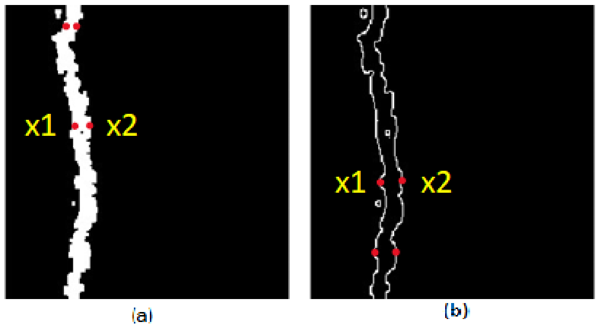

Figure 13. Pixel coordinates in the (a) edge image and (b) segmentation.

Figure 14. Crack width.

5.6.2. Crack width

Feature extraction is a multi-step procedure that includes binarization, picture separation, and feature pixel counting. Initially, the image is transformed into a binary representation. Here, the images are split into four horizontal and four vertical sections. Each area of the binarized image is then tallied using white pixels (56, 57). These pixel counts are used as fracture categorization features (6). Selecting two places on the picture and measuring the distance in millimeters between them allows for the calculation of the calibration factor. Figure 13 shows the pixel co-ordinates of the boundary points. The crack widths observed in our study, ranging from 0.2 to 7.22 pixels, are similar to those reported by Carrasco et al., with measurements between 2 and 14.7 pixels (58, 59).

The calculation of this component involves dividing the actual length by the pixel length. The height of the image in the event of a vertical fracture or its width in the case of a horizontal crack is then traversed using a loop. Each time the loop is iterated, the distances are calculated and maintained in an array (48). The relationship between the maximum distance of the crack and its greatest width is then determined, and this correlation provides a width measurement. This procedure makes it easier to locate the crack and capture images, while indicating the known length of each image. Figure 14 show that this method provides precise measurements and the categorization of cracks based on their diameters through calibration and extracting their characteristics. Table 4 displays the evaluation of crack width and length of concrete surface.

Table 4. Detection of crack width and crack length.

S.No	Captured image	Image processed using MATLAB	Crack width (pixels)	Crack width (mm)	Crack length (pixels)	Crack length (mm)
1 layer for 25% of the applied load		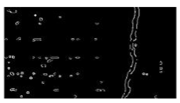	Min: 3 Max: 21	0.79 5.51	221	58
2 layers for 25% of the applied load		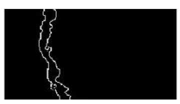	Min: 3 Max: 24	0.79 6.5	207	55.5

1 layer for 50% of the applied load	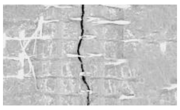	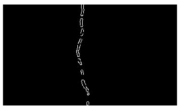	Min: 1 Max: 16	0.2 4.54	202	53.2
2 layers for 50% of the applied load			Min: 1 Max: 26	0.2 7	215	57
1 layer for full failure		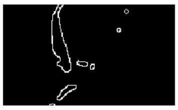	Min: 1 Max: 29	0.2 7.22	198	52.55
2 layers for full failure		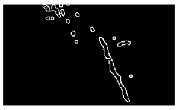	Min: 3 Max: 19	0.79 5.12	220	58.2

6. CONCLUSIONS

In this study, a 3D FEM was developed to examine the behavior of concrete beams reinforced with FRCM. The following conclusions were drawn from this study are as follow:

• Finite element analysis was used to predict the behavior of the damaged and strengthened concrete beams. Finite element analyses were helpful in examining the effects of the various components of the FRP composites.

• The use of glass-FRCMs enhanced the load-carrying capacity of the un-strengthened concrete beams by approximately 41%.

• The beam pre-loaded with 25% attained a maximum load of 9.84kN, which was 22.4% higher than that of the un-strengthened beam for single layers. For two and three layers, the load was increased up to 25.12% and 50%, respectively.

• By increasing the damage level to 50%, the maximum load increased to 7.59%, 14.18%, and 41.04%, and the 100% pre-loaded beam, increased in strength by approximately 2.73% and 11.04%, respectively.

• Finite element analysis was performed by applying the loading capacity method. Using this method, the deflection value was approximately 10%10% lower than the experimental results.

• The crack identification and crack feature measurement techniques recommended in this study demonstrate remarkable performance and accuracy with high computational efficiency.

• FEM can be used for both the design of concrete structures and assessing the long-term behavior of the structures to determine their strength, dependability, and remaining life, as well as for strengthening and continued.

Abbreviations

FRCM – Fabric - Reinforced Cementitious Matrix; FRP – Fiber Reinforced polymer; PVA - Polyvinyl alcohol; SF - Silica fume; SCBA - Sugarcane bagasse ash; FEA - Finite element analysis; FEM- Finite element model, GF - Glass fabric.

Availability of data and material

The data will be available on request.

Acknowledgements

Authors would like to acknowledge the Management and Dean-School of Civil Engineering, Vellore Institute of Technology, Chennai, India for providing the necessary support to carry out this research.

Authorship contribution statement

R. Kirthiga: Conceptualization, Investigation, Methodology, Writing-original draft, software, Validation.

Saravanan Hariny: Data Curation.

Remin Javad: Formal analysis, Software.

S. Elavenil: Supervision, Writing-review & editing.

Declaration of competing interest

The authors of this article declare that they have no financial, professional or personal conflicts of interest that could have inappropriately influenced this work.

REFERENCES

1. Mandor A, El Refai A. 2022. Strengthening the hogging and sagging regions in continuous beams with fiber-reinforced cementitious matrix (FRCM): Experimental and analytical investigations. Constr. Build. Mater. 321:126341. https://doi.org/10.1016/j.conbuildmat.2022.126341
2. Guo L, Deng M, Hui Chen, Ruizhe Li, Xiangkun Ma, Yangxi Zhang. 2022. Experimental study on pre-damaged RC beams shear-strengthened with textile-reinforced mortar (TRM). Eng. Solid Mech. 256:113956. https://doi.org/10.1016/j.engstruct.2022.113956
3. Natraj K, Kirthiga R, Elavenil S. 2023. Structural performance of RCC building and strengthening the structural members with CFRP. Mater. Today Proc. 84:24-32. https://doi.org/10.1016/j.matpr.2023.04.304
4. Yu F, Guo S, Wang S, Fang Y. 2019. Experimental study on high pre-cracked RC beams shear-strengthened with CFRP strips. Compos. Struct. 225:111163. https://doi.org/10.1016/j.compstruct.2019.111163
5. Rajkumar PRK, Jilani S, Sudha C, Jegan M, Sundararaj JB. 2021. Flexural performance of textile reinforced concrete with hybrid fabric mesh. ARPN J. Eng. Appl. Sci. 16(20):2132–2140.
6. Kirthiga R, Elavenil S. 2022. A review on using inorganic binders in fiber reinforced polymer at different conditions to strengthen reinforced concrete beams. Constr. Build. Mater. 352:129054. https://doi.org/10.1016/j.conbuildmat.2022.129054
7. Kirthiga R, Elavenil S. 2024. Performance evaluation of pre-damaged reinforced concrete beams strengthened with knitted glass fabric reinforced cementitious matrix: Flexure and shear behaviors. Structures. 70:107744. https://doi.org/10.1016/j.istruc.2024.107744
8. Tetta ZC, Bournas DA. 2016. TRM Vs FRP jacketing in shear strengthening of concrete members subjected to high temperatures. Compos. Part B. 106:190–205. https://doi.org/10.1016/j.compositesb.2016.09.026
9. Koutas LN, Tetta Z, Bournas DA, Triantafillou TC. 2019. Strengthening of Concrete structures with textile reinforced mortars: State-of-the-art review. J. Compos. Constr. 23(1):1–20. https://doi.org/10.1061/(ASCE)CC.1943-5614.0000882. https://doi.org/10.1061/(ASCE)CC.1943-5614.0000882
10. Giese ACH, Giese DN, Dutra VFP, Pinto Da Silva Filho LC. 2021. Flexural behavior of RC beams strengthened with textile reinforced concrete. Adv. Struct. Mech. Appl. 26:213-225. https://doi.org/10.1007/978-3-031-05509-6_18
11. Dong Z, Deng M, Dai J, Song S. 2021. Flexural strengthening of RC slabs using textile reinforced mortar improved with short PVA fibers. Constr. Build. Mater. 304:124613. https://doi.org/10.1016/j.conbuildmat.2021.124613
12. Sabbaghian M, Kheyroddin A. 2020. Flexural strengthening of RC one way slabs with high-performance fiber-reinforced cementitious composite laminates using steel and GFRP bar. Eng. Struct. 221:111106. https://doi.org/10.1016/j.engstruct.2020.111106
13. Tello N, Alhoubi Y, Abed F, El Refai A, El-Maaddawy T. 2021. Circular and square columns strengthened with FRCM under concentric load. Compos. Struct. 255:113000. https://doi.org/10.1016/j.compstruct.2020.113000
14. Faleschini F, Zanini MA, Hofer L, Pellegrino C. 2020. Experimental behavior of reinforced concrete columns confined with carbon-FRCM composites. Constr. Build. Mater. 243:118296. https://doi.org/10.1016/j.conbuildmat.2020.118296
15. Guo L, Deng M, Li T. 2023. Seismic behaviour of RC columns retrofitted with textile-reinforced mortar TRM. optimized by short PVA fibres. Structures. 50:244–254. https://doi.org/10.1016/j.istruc.2023.02.041
16. Koutas LN, Papakonstantinou CG. 2021. Flexural strengthening of RC beams with textile-reinforced mortar composites focusing on the influence of the mortar type. Eng. Struct. 246:113060. https://doi.org/10.1016/j.engstruct.2021.113060
17. Tetta ZC, Koutas LN, Bournas DA. 2015. Textile-reinforced mortar TRM. versus fiber-reinforced polymers FRP. in shear strengthening of concrete beams. Compos. Part B Eng. 77:338–348. https://doi.org/10.1016/j.compositesb.2015.03.055
18. Ombres L. 2011. Flexural analysis of reinforced concrete beams strengthened with a cement based high strength composite material. Compos. Struct. 94(1):143–155. https://doi.org/10.1016/j.compstruct.2011.07.008
19. D'Ambrisi A, Focacci F. 2011. Flexural strengthening of RC beams with cement-based composites. J. Compos. Constr. 15(5):707–720. https://doi.org/10.1061/(asce)cc.1943-5614.0000218
20. Babaeidarabad S, Loreto G, Nanni A. 2014. Flexural strengthening of RC beams with an externally bonded fabric-reinforced cementitious matrix. J. Compos. Constr. 18(5):04014009. https://doi.org/10.1061/(ASCE)CC.1943-5614.0000473
21. Ebead U, Shrestha KC, Afzal MS, El Refai A, Nanni A. Effectiveness of fabric-reinforced cementitious matrix in strengthening reinforced concrete beams. J. Compos. Constr. 21(2):04016084. https://doi.org/10.1061/(asce)cc.1943-5614.0000741
22. El-Maaddawy T, El Refai A. 2016. Innovative repair of severely corroded t-beams using fabric-reinforced cementitious matrix. J. Compos. Constr. 20(3):04015073. https://doi.org/10.1061/(asce)cc.1943-5614.0000641

23. Awani O, El-Maaddawy T, El Refai A. 2016. Numerical simulation and experimental testing of concrete beams strengthened in shear with fabric-reinforced cementitious matrix. J. Compos. Constr. 20(6):04016056. https://doi.org/10.1061/(asce)cc.1943-5614.0000711
24. Loreto G, Leardini L, Arboleda D, Nanni A. 2014. Performance of RC Slab-type elements strengthened with fabric-reinforced cementitious-matrix composites. J. Compos. Constr. 18(3):1–9. https://doi.org/10.1061/(asce)cc.1943-5614.0000415
25. D'Ambrisi A, Feo L, Focacci F. 2013. Experimental and analytical investigation on bond between Carbon-FRCM materials and masonry. Compos. Part B Eng. 46:15–20. https://doi.org/10.1016/j.compositesb.2012.10.018
26. Zheng YZ, Wang WW, Brigham JC. 2016. Flexural behaviour of reinforced concrete beams strengthened with a composite reinforcement layer: BFRP grid and ECC. Constr. Build. Mater. 115:424–437. https://doi.org/10.1016/j.conbuildmat.2016.04.038
27. Jafarzadeh H, Nematzadeh M. 2022. Flexural strengthening of fire-damaged GFRP-reinforced concrete beams using CFRP sheet: Experimental and analytical study. Compos. Struct. 288:115378. https://doi.org/10.1016/j.compstruct.2022.115378
28. Pandiyan T, Solaiyan E. 2024. Effect of zinc industrial waste on the mechanical and microstssructural properties of the ternary blended concrete. Glob. Nest. J. 26(10):1-8. https://doi.org/10.30955/gnj.005555
29. Pandiyan T, Solaiyan E. 2024. A comparative study of jarosite and other cementitious materials as a concrete material-A review. Eng. Appl. Sci. Res. 51:376–392. Retrieved from https://ph01.tci-thaijo.org/index.php/easr/article/view/254390
30. Mohan A, Poobal S. 2018. Crack detection using image processing: A critical review and analysis. Alexandria Eng. J. 57(2):787–798. https://doi.org/10.1016/j.aej.2017.01.020
31. Kirthiga R, Elavenil S. 2024. A survey on crack detection in concrete surface using image processing and machine learning. J. Build. Pathol. Rehabil. 9:15. https://doi.org/10.1007/s41024-023-00371-6
32. Liu X, Ai Y, Scherer S. 2017. Robust image-based crack detection in concrete structure using multi-scale enhancement and visual features. IEEE International Conference on Image Processing (ICIP), Beijing, China, 2017, pp. 2304-2308. pp 2304–2308. https://doi.org/10.1109/ICIP.2017.8296693
33. Senin SF, Yusuff A, Rohim R, Chan HB. 2023. Reinforced concrete surface cracks length detection and length estimation by using digital image processing approach. IOP Conf. Ser. Earth. Environ. Sci. 1238:012003. https://doi.org/10.1088/17551315/1238/1/012003
34. Su C, Wang W. 2020. Concrete cracks detection using convolutional neuralnetwork based on transfer learning. Math. Probl. Eng. 2020:7240129 https://doi.org/10.1155/2020/7240129
35. Broberg P. 2013. Surface crack detection in welds using thermography. NDT E Int. 57:69–73. https://doi.org/10.1016/j.ndteint.2013.03.008
36. Shan B, Zheng S, Ou J. 2016. A stereovision-based crack width detection approach for concrete surface assessment. KSCE J. Civ. Eng. 20:803–812. https://doi.org/10.1007/s12205-015-0461-6
37. Li G, Xiao X, Gui Y. 2009. A novel algorithm of image denoising based on the grey absolute relational analysis. 2009 IEEE Int Conf. Grey. Syst. Intell. Serv. GSIS 2009 181–185. https://doi.org/10.1109/GSIS.2009.5408327
38. Jahanshahi MR, Masri SF. 2013. A new methodology for non-contact accurate crack width measurement through photogrammetry for automated structural safety evaluation. Smart. Mater. Struct. **22**:035019. https://doi.org/10.1088/0964-1726/22/3/035019
39. Kirthiga R, Elavenil S. 2023. Potential utilization of sugarcane bagasse ash in cementitious composites for developing inorganic binder. Ain. Shams. Eng. J. 14(11):102560. https://doi.org/10.1016/j.asej.2023.102560
40. IS-10262:2019. Concrete mix proportioning - guidelines (second revision). bureau of indian standard.
41. Banjara NK, Ramanjaneyulu K. 2019. Investigations on behaviour of flexural deficient and CFRP strengthened reinforced concrete beams under static and fatigue loading. Constr. Build. Mater. 201:746–762. https://doi.org/10.1016/j.conbuildmat.2019.01.010
42. Tan C, Sun T, Zhao H, Tu L, Qiao D, Shao X. 2024. Shear behavior of pre-damaged RC beams strengthened with steel plate and UHPC. J. Constr. Steel. Res. 212:108287. https://doi.org/10.1016/j.jcsr.2023.108287
43. Koutas LN, Bournas AD. 2016. Flexural strengthening of two-way RC slabs with textile-reinforced mortar: experimental investigation and design equations. J. Compos. Cons. 21(1):1-34. https://doi.org/10.1061/(ASCE)CC.1943-5614.0000713
44. ISO-10534-1-1996. International standard 2004. carbon fibre - determination of tensile properties of resin-impregnated yarn. Int. Organ. Stand. 10406–1:20 (2015) 3–6.
45. Revanna N, Moy CKS 2023. Numerical modelling of reinforced concrete flexural members strengthened using textile reinforced mortars. Front. Struct. Civ. Eng. 17:649–668. https://doi.org/10.1007/s11709-023-0919-4
46. Wang P, Huang H. 2010. Comparison analysis on present image-based crack detection methods in concrete structures. In: Proc. 2010 3rd Int. Congr. Image Signal Process. CISP 2010. 2530–2533. https://doi.org/10.1109/CISP.2010.5647496
47. Mir BA, Sasaki T, Nakao K, Nagae K, Nakada K, Mitani M, Tsukada T, Osada N, Terabayashi K, Jindai M. 2022. Machine learning-based evaluation of the damage caused by cracks on concrete structures. Precis. Eng. 76:314–327. https://doi.org/10.1016/j.precisioneng.2022.03.016
48. Golding VP, Gharineiat Z, Munawar HS, Ullah F. 2022. Crack detection in concrete structures using deep learning. Sustain. 14(13):8117. https://doi.org/10.3390/su14138117
49. Jayajothi P, Kumutha Rathinam R, Vijai K. 2013. Finite element analysis of FRP strengthened RC beams using ansys. Asian J. Civ. Eng. 14:631–642.

50. Bouziadi F, Boulekbache B, Haddi A, Hamrat M, Djelal C. 2020. Finite element modeling of creep behavior of FRP-externally strengthened reinforced concrete beams. Eng. Struct. 204:109908. https://doi.org/10.1016/j.engstruct.2019.109908
51. Mustapha YG, Halliru AM, Hobon FA, Aibinu A, Thomas S, Malami NS. 2021. Crack detection on surfaces using digital image processing. 2021 1st. Int. Conf. Multidiscip. Eng. Appl. Sci. ICMEAS 2021:1-6. https://doi.org/10.1109/ICMEAS52683.2021.9692367
52. Kim H, Ahn E, Shin M, Sim SH. 2019.Crack and noncrack classification from concrete surface images using machine learning. Struct. Heal. Monit. 18(3):725–738. https://doi.org/10.1177/1475921718768747
53. Madiha Z, Syed A, Wakeel A, Farrukh ZK. 2021. Structural crack detection and classification using deep convolutional neural network. Pakistan J. Eng. Technol. 4(4):50–60. https://doi.org/https://doi.org/10.51846/vol4iss4pp50-56
54. Adhikari RS, Moselhi O, Bagchi A. 2012. Image-based retrieval of concrete crack properties. 2012 Proc 29th Int. Symp. Autom. Robot. Constr. ISARC 2012. https://doi.org/10.22260/isarc2012/0054
55. Munawar HS, Hammad AWA, Haddad A, Soares CAP, Waller ST. 2021. Image-based crack detection methods: A review. Infrastructures. 6(8):115. https://doi.org/10.3390/infrastructures6080115
56. Jawdhari A, Adheem AH, Kadhim MMA. 2020. Parametric 3D finite element analysis of FRCM-confined RC columns under eccentric loading. Eng. Struct. 212:110504. https://doi.org/10.1016/j.engstruct.2020.110504
57. Aravind N, Nagajothi S, Elavenil S. 2021. Machine learning model for predicting the crack detection and pattern recognition of geopolymer concrete beams. Constr. Build. Mater. 297:123785. https://doi.org/10.1016/j.conbuildmat.2021.123785
58. Miguel C, Araya letelier Gerardo, Ramiro V, Paolo V. 2021. Image-based automated width measurement of surface cracking. Sensors Switzerland. *21*(22):7534. https://doi.org/10.3390/s21227534
59. Prasanna P, Dana KJ, Gucunski N, Basily BB, La HM, Lim RS, Parvardeh H. 2016. Automated crack detection on concrete bridges. IEEE Trans. Autom. Sci. Eng. 13(2):591–599. https://doi.org/10.1109/TASE.2014.2354314